Supplement of Adv. Stat. Clim. Meteorol. Oceanogr., 11, 273–292, 2025 https://doi.org/10.5194/ascmo-11-273-2025-supplement © Author(s) 2025. CC BY 4.0 License.





Supplement of

Soil moisture–temperature coupling during extreme warm conditions in 2018 in Sweden: a case study with WRF-CTSM

Iris Mužić et al.

Correspondence to: Iris Mužić (iris.muzic@cicero.oslo.no)

The copyright of individual parts of the supplement might differ from the article licence.

Sect. S1.

Unit conversions

In situ surface volumetric soil water content is compared to the surface soil moisture from the gridded datasets using:

$$VWC = \frac{SWC}{100}$$
 (S1)

where VWC is the volumetric water content (mm³ mm⁻³), and SWC is the soil water content (%).

Evaporation and latent heat are both utilized in this study. The conversion between them is performed using:

$$E = \frac{LH}{\lambda}$$
 (S2)

$$\lambda = (2.501 - 0.00237 * T) \times 10^6$$

where E is evaporation (kg m⁻² s⁻¹), LH is latent heat flux (W m⁻²), λ is the latent heat of vaporization (J kg⁻¹), and T is the air temperature at 2 m height (°C) (Allen et al., 1998).

In the case of WRF-CTSM latent heat output conversion to evaporation, the air temperature from the corresponding model time step is utilized in Eq. S2, and if GLEAM evaporation is converted to latent heat, a default air temperature of 20 °C is used since the latent heat of vaporization varies only slightly with temperature.

Sect. S2.

Evaluation metrics

The equations for the calculation of the Pearson correlation coefficient (PCC), root mean square error (RMSE), and absolute bias (AB) are provided below.

$$PCC = \frac{\sum_{i=1}^{n} (M_i - \bar{M})(O_i - \bar{O})}{\sqrt{\sum_{i=1}^{n} (M_i - \bar{M})^2} \sqrt{\sum_{i=1}^{n} (O_i - \bar{O})^2}}$$
(S3)

RMSE =
$$\sqrt{\frac{1}{n}\sum_{i=1}^{n}(M_i - O_i)^2}$$
 (S4)

$$AB = \overline{M} - \overline{O} \tag{S5}$$

In the equations above,

M is the modeled data,

0 is the observed data,

 \overline{M} is the mean of the modeled data,

 \bar{O} is the mean of the observed data,

n is the total number of observations,

 M_i is the *i*th value of the modeled data,

 O_i is the *i*th value of the observed data.

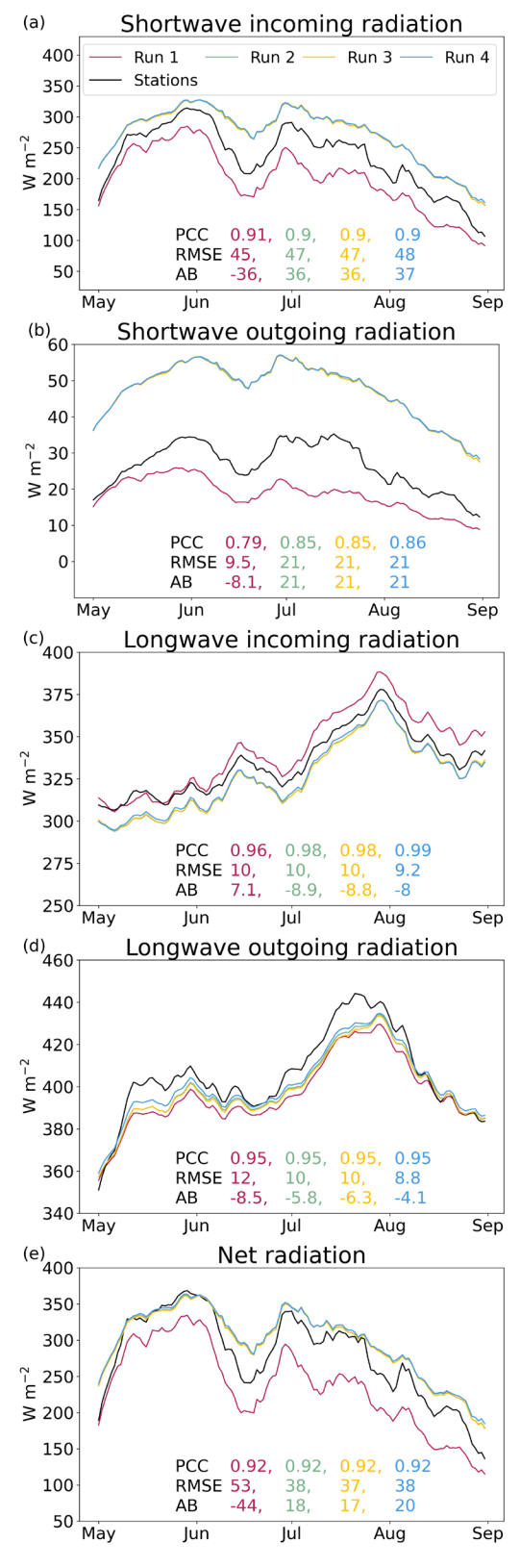


Figure S1. Grid cell level evaluation of WRF-CTSM simulations against *in situ* observations averaged over three stations (Norunda, Hyltemossa, and Degerö) during MJJA 2018, illustrated as a 10-day centered running mean time series. Evaluation metrics are based on daily values and calculated relative to the station data. They include the Pearson correlation coefficient (PCC), root mean square error (RMSE), and absolute bias (AB).

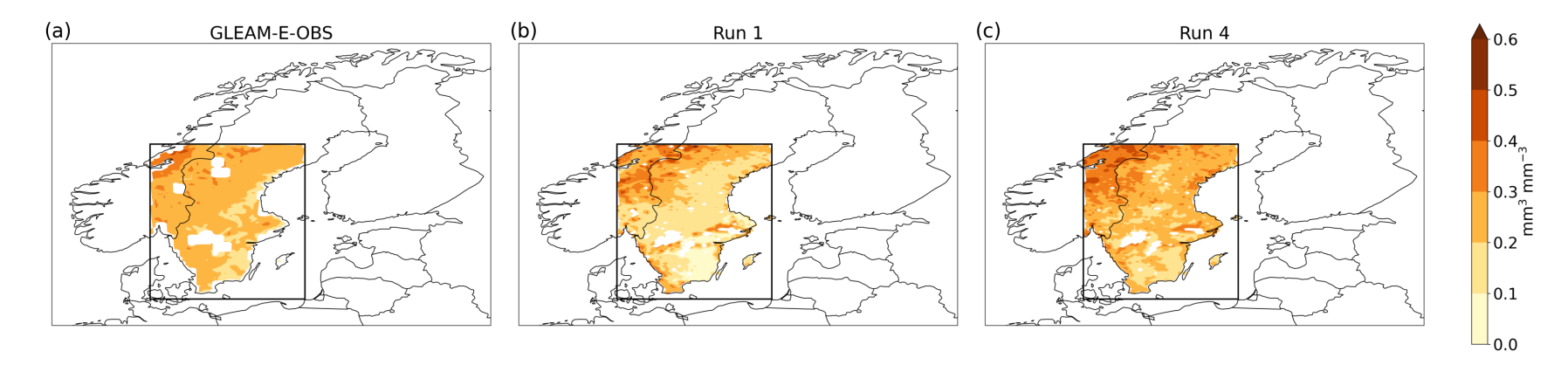


Figure S2. Mean regional MJJA 2018 surface soil moisture in a) GLEAM-E-OBS, b) Run 1, and c) Run 4.

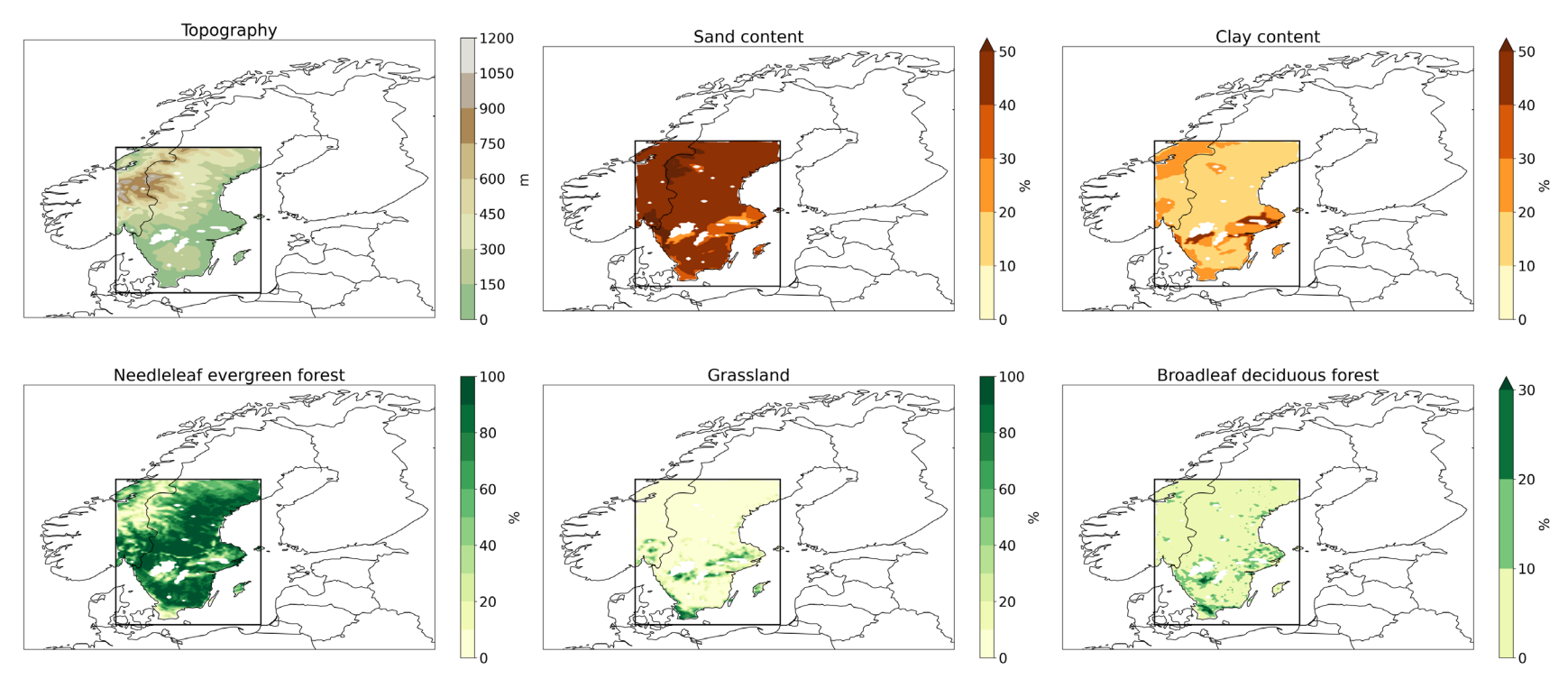


Figure S3. Land surface characteristics of the study domain used in WRF-CTSM simulations. Percentages indicate the proportion of each model grid cell (0.1° grid spacing) occupied by the respective land surface properties. Topography is derived from an elevation dataset at 1 km resolution (Verdin and Greenlee, 1996). Soil texture represents the uppermost soil layer (0–0.1 m depth) and is sourced from a dataset with a 0.083° resolution (Global Soil Data Task, 2000). The bottom row presents dominant vegetation types in the study area obtained from a dataset on a 0.05° resolution (Lawrence and Chase, 2007). Needleleaf evergreen forest vegetation combines the needleleaf temperate and boreal evergreen forest plant functional types (PFTs), while broadleaf deciduous forest combines the broadleaf temperate and boreal deciduous forest PFTs. Grassland refers to the C3 grasses PFT in WRF-CTSM.

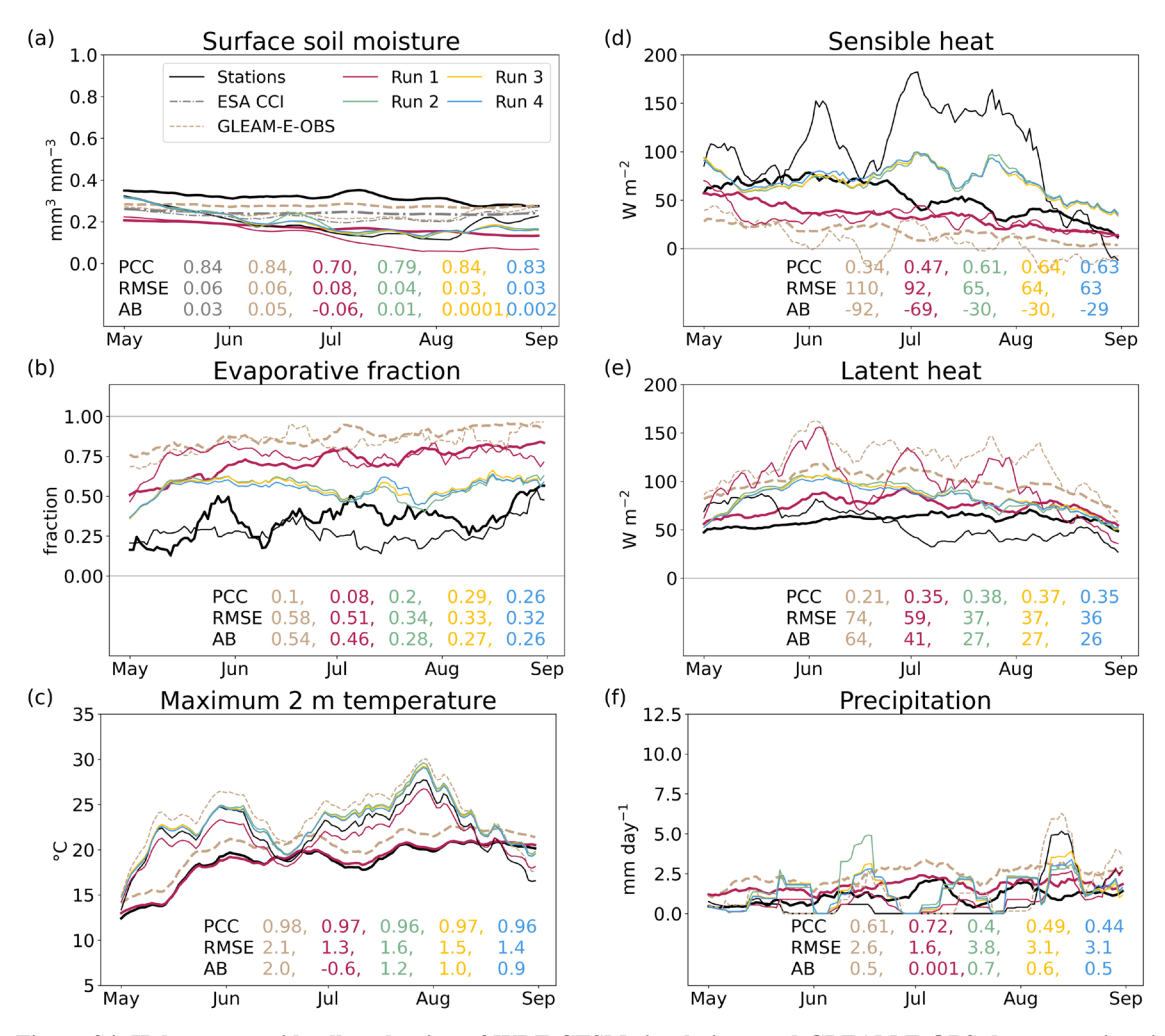


Figure S4. Hyltemossa grid cell evaluation of WRF-CTSM simulations and GLEAM-E-OBS dataset against *in situ* observations, illustrated as a 10-day centered running mean time series. Thin lines represent MJJA 2018, while thick lines (stations, ESA CCI, GLEAM-E-OBS, and Run 1) denote the mean of the other available years for which *in situ* data are available, 2015–2020, excluding the year 2018. Key soil moisture–temperature coupling variables are evaluated in panels a–c. Surface soil moisture depths are 0.05 m (ESA CCI) and 0.1 m (stations, GLEAM-E-OBS, and Runs 1–4). Evaporative fraction values are constrained between 0 and 1. Evaluation metrics in the bottom right are for daily values during MJJA 2018 and calculated relative to the station data. They include the Pearson correlation coefficient (PCC), root mean square error (RMSE), and absolute bias (AB).

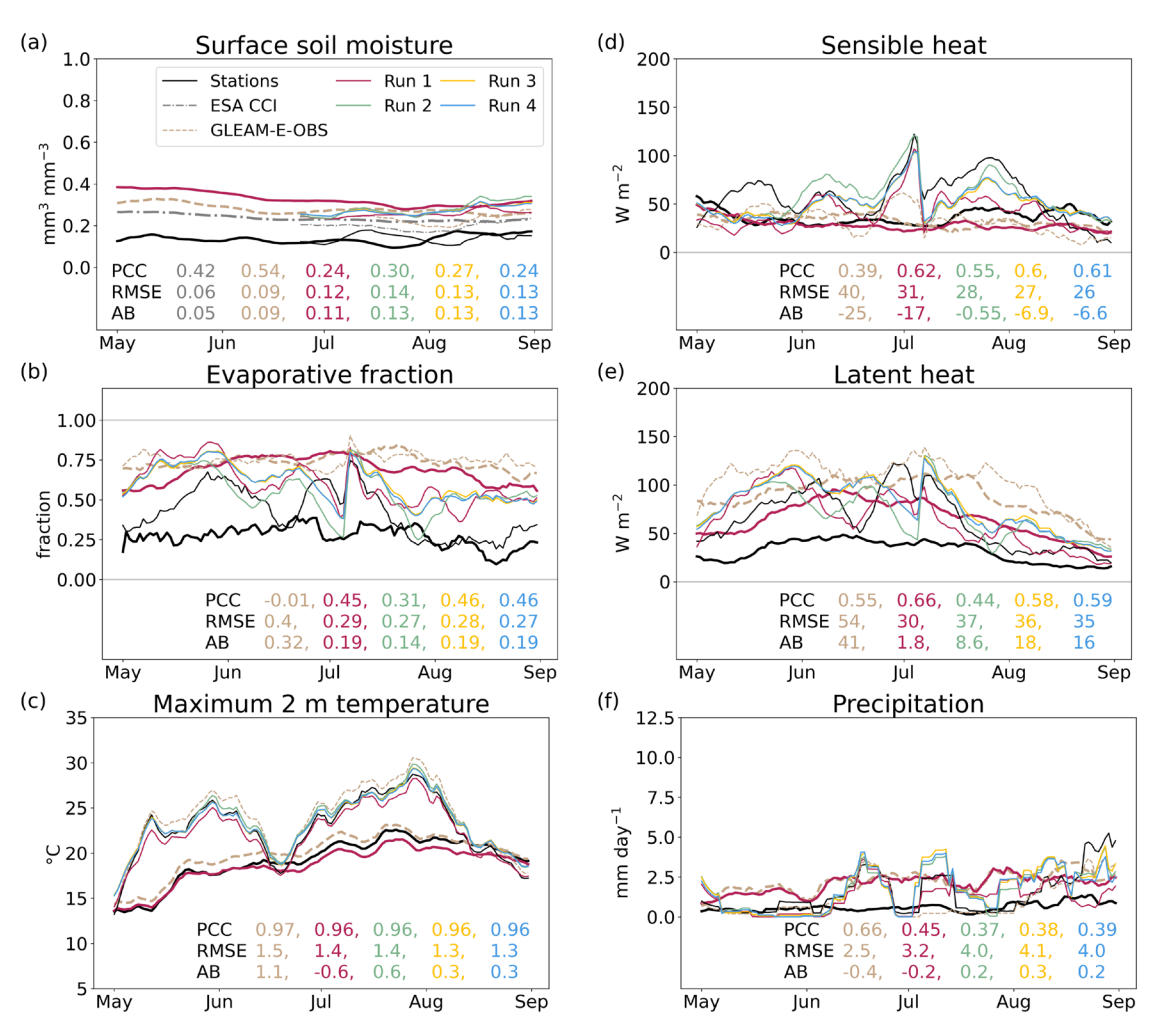


Figure S5. As in Fig. S4, but for Lanna. Thick lines denote the mean of the other available years for which *in situ* data are available, 2014–2018, excluding the year 2018.

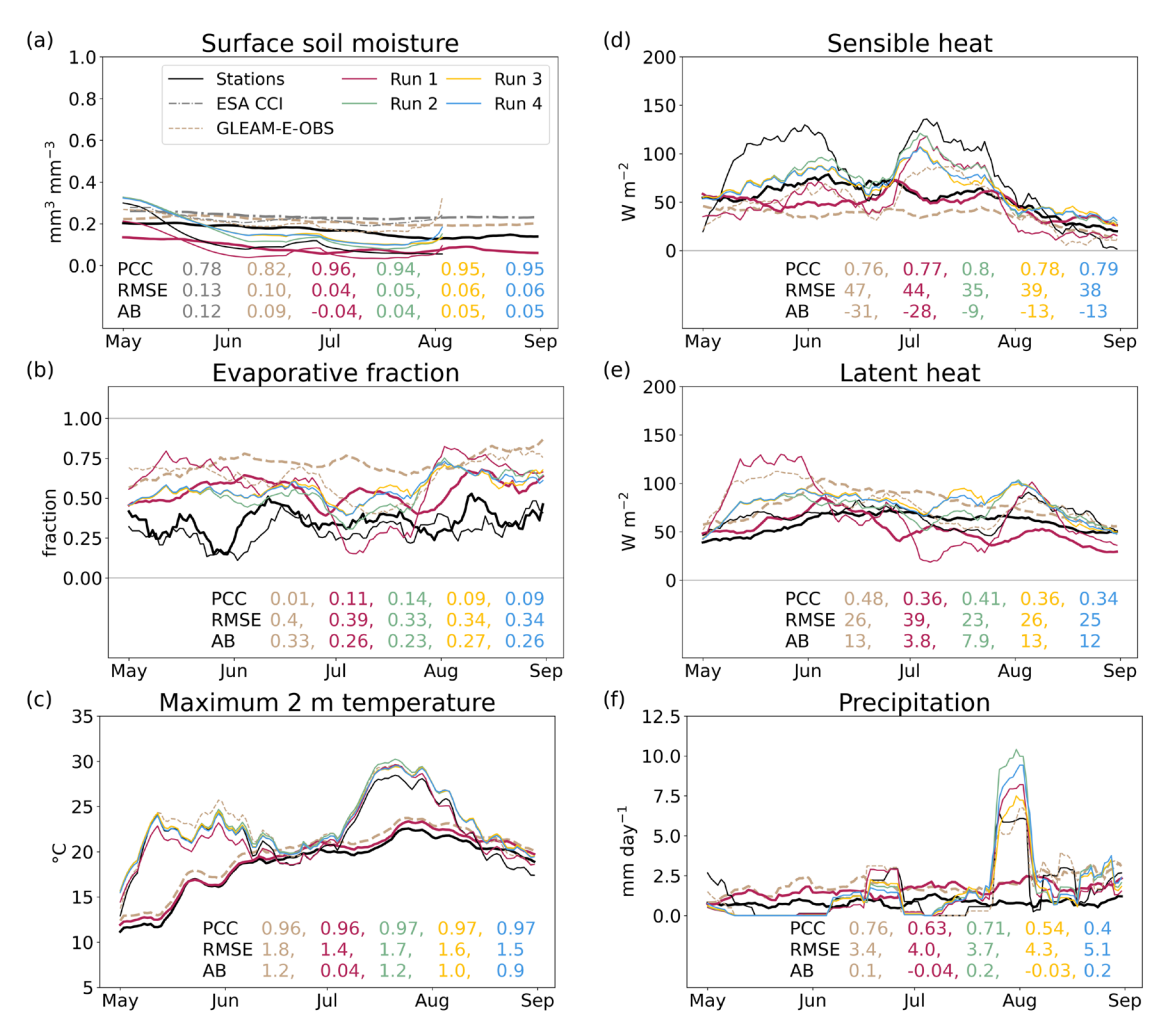


Figure S6. As in Fig. S4, but for Norunda. Thick lines denote the mean of the other available years for which *in situ* data are available, 2014–2020, excluding the year 2018.

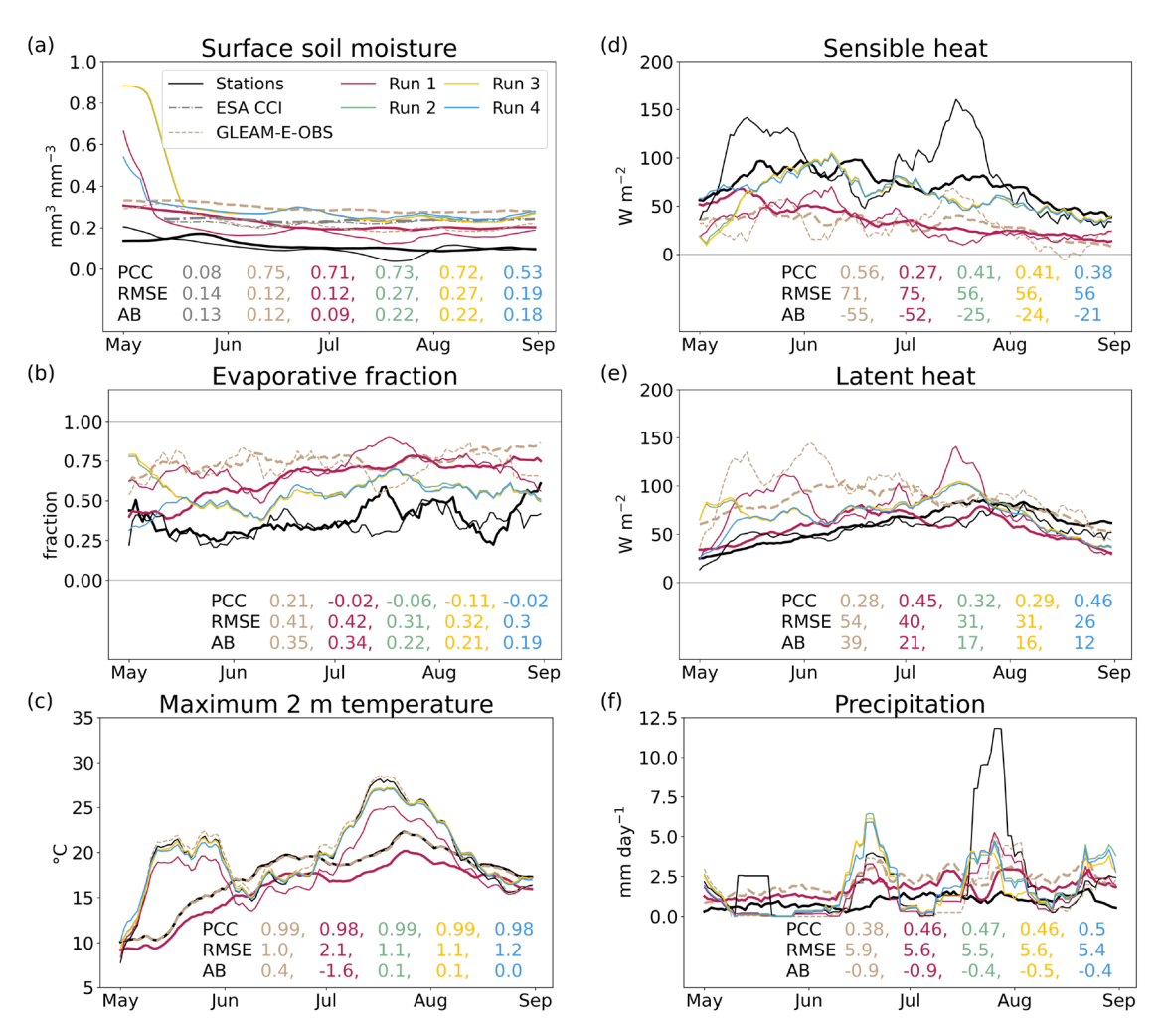


Figure S7. As in Fig. S4, but for Rosinedal-3. Thick lines denote the mean of the other available years for which *in situ* data are available, 2014–2020, excluding the year 2018.

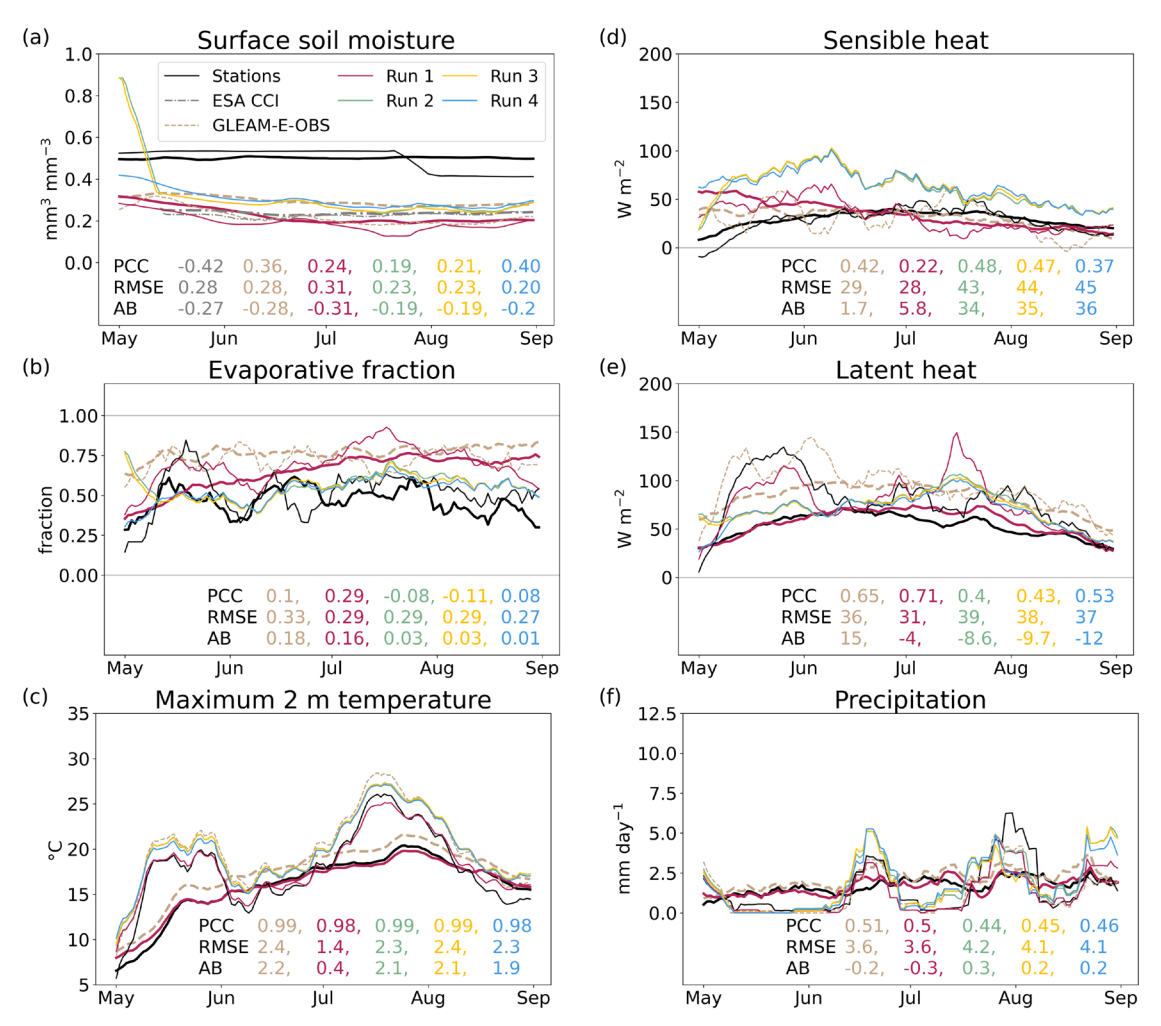


Figure S8. As in Fig. S4, but for Degerö. Thick lines denote the mean of the other available years for which *in situ* data are available, 2014–2020, excluding the year 2018.

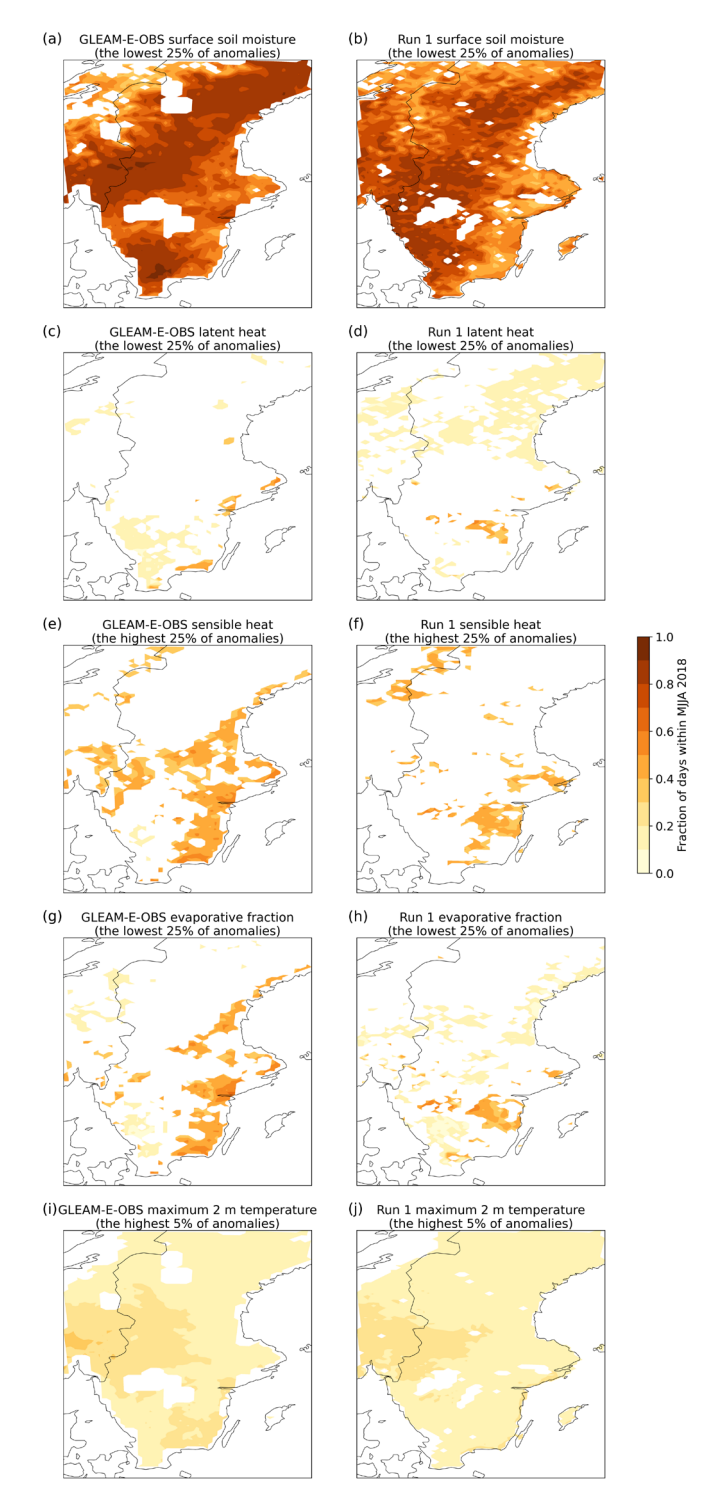


Figure S9. Fraction of days during MJJA 2018 when daily anomalies fall beyond the selected percentile thresholds, computed relative to the anomaly distribution from MJJA 2010–2022 (excluding 2018), shown for GLEAM-E-OBS (left column) and Run 1 (right column). For each grid cell, the percentile threshold of the reference period distribution is first calculated. The 2018 daily anomalies are then compared against this threshold, and the fraction of days above/below the threshold is computed. Grid cells where the fraction significantly differs from the theoretical expectation (based on a chi-squared test at the 99% confidence level) are colored, as also done in Dirmeyer et al. (2021). For example, grid cells where 1/3 of all MJJA 2018 days fall within the highest 5% of daily T_{MAX} anomalies relative to MJJA 2010–2022 (excluding the year 2018) indicate that anomalously very high T_{MAX} persisted 41 days at those locations.

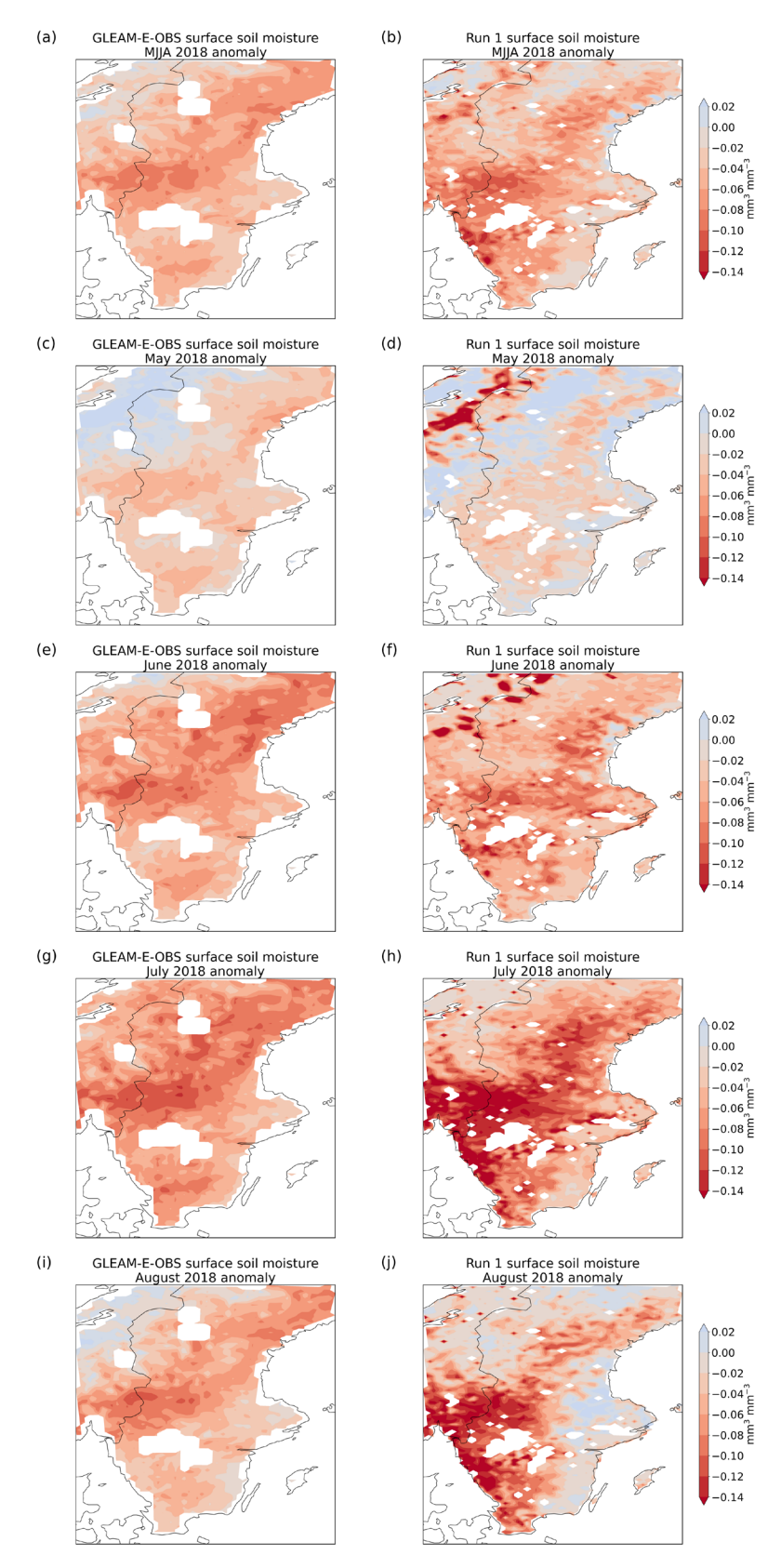


Figure S10. Mean seasonal and monthly May-August anomalies in surface soil moisture in GLEAM-E-OBS (left column) and Run 1 (right column).

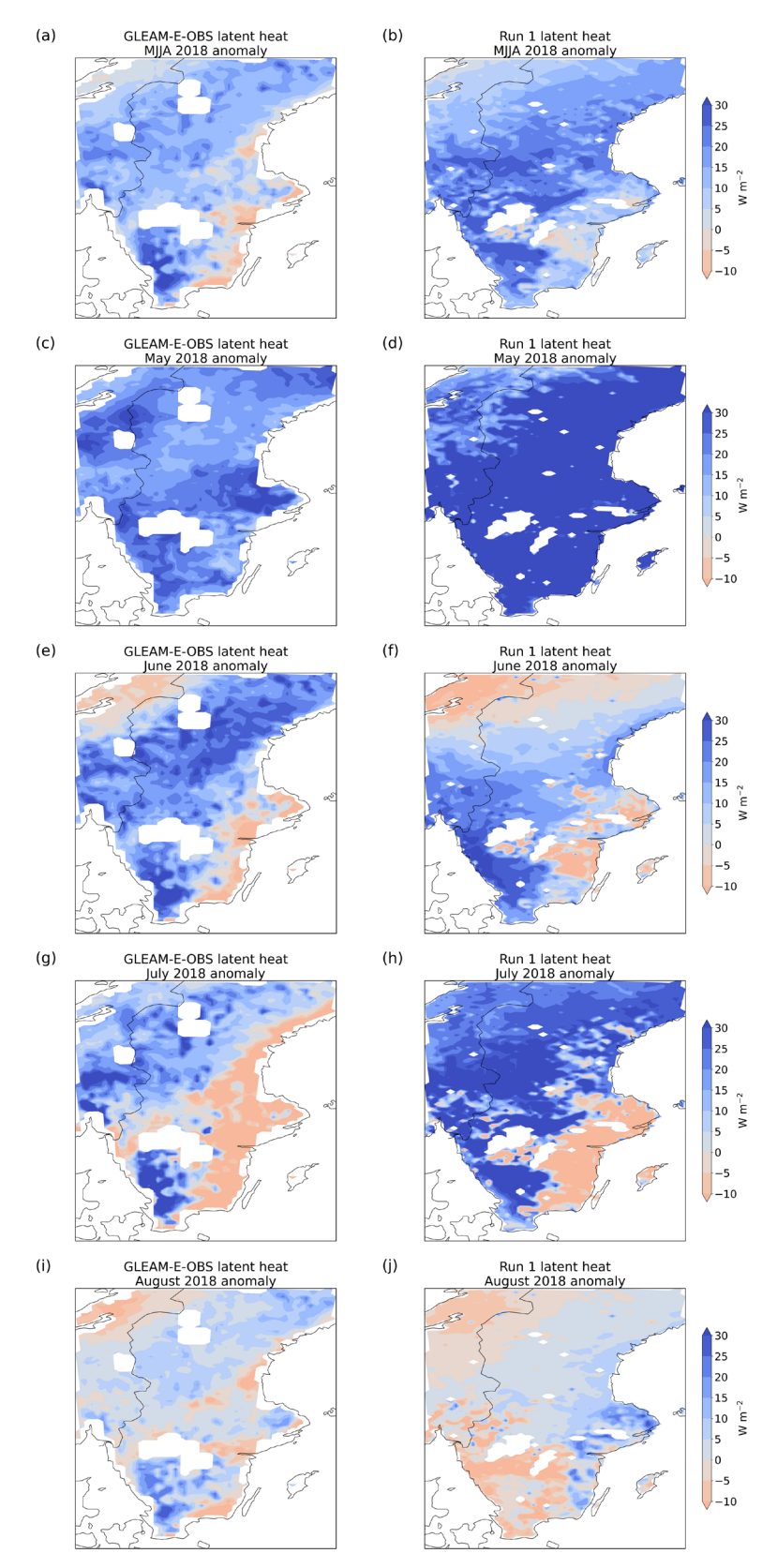


Figure S11. Mean seasonal and monthly May-August anomalies in latent heat in GLEAM-E-OBS (left column) and Run 1 (right column).

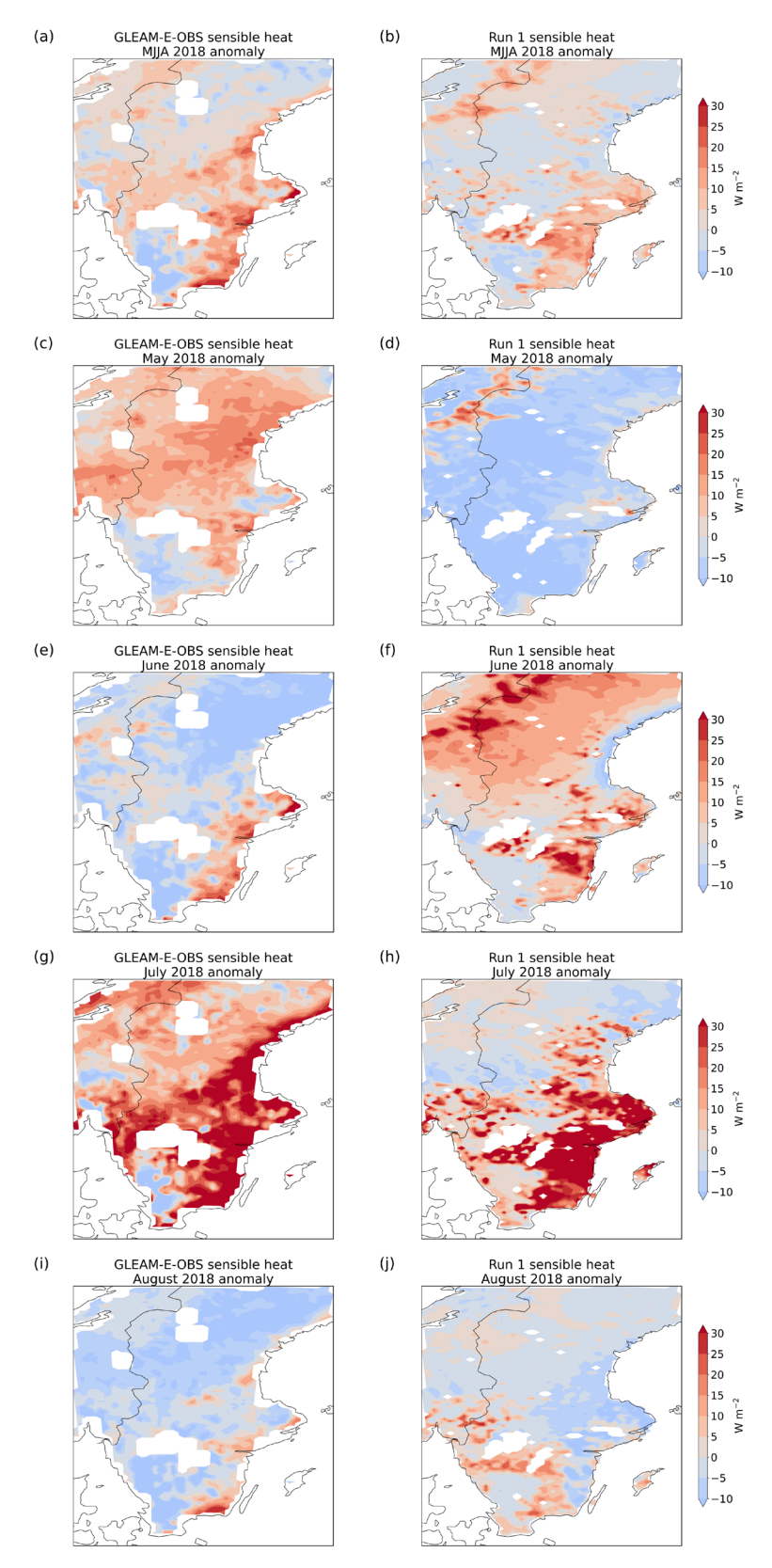
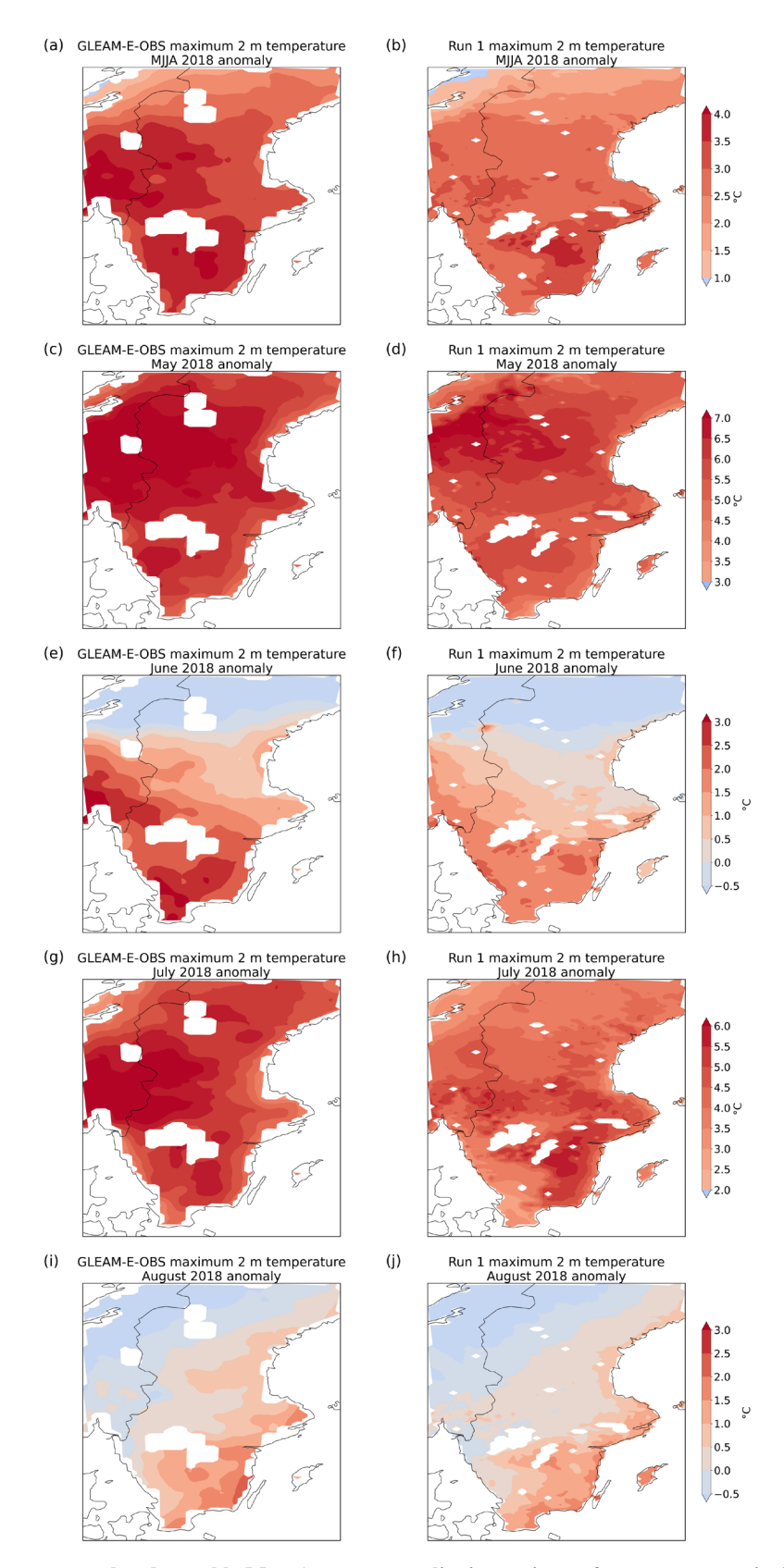


Figure S12. Mean seasonal and monthly May-August anomalies in sensible heat in GLEAM-E-OBS (left column) and Run 1 (right column).



Figure~S13.~Mean~seasonal~and~monthly~May-August~anomalies~in~maximum~2~m~temperature~in~GLEAM-E-OBS~(left~column)~and~Run~1~(right~column).

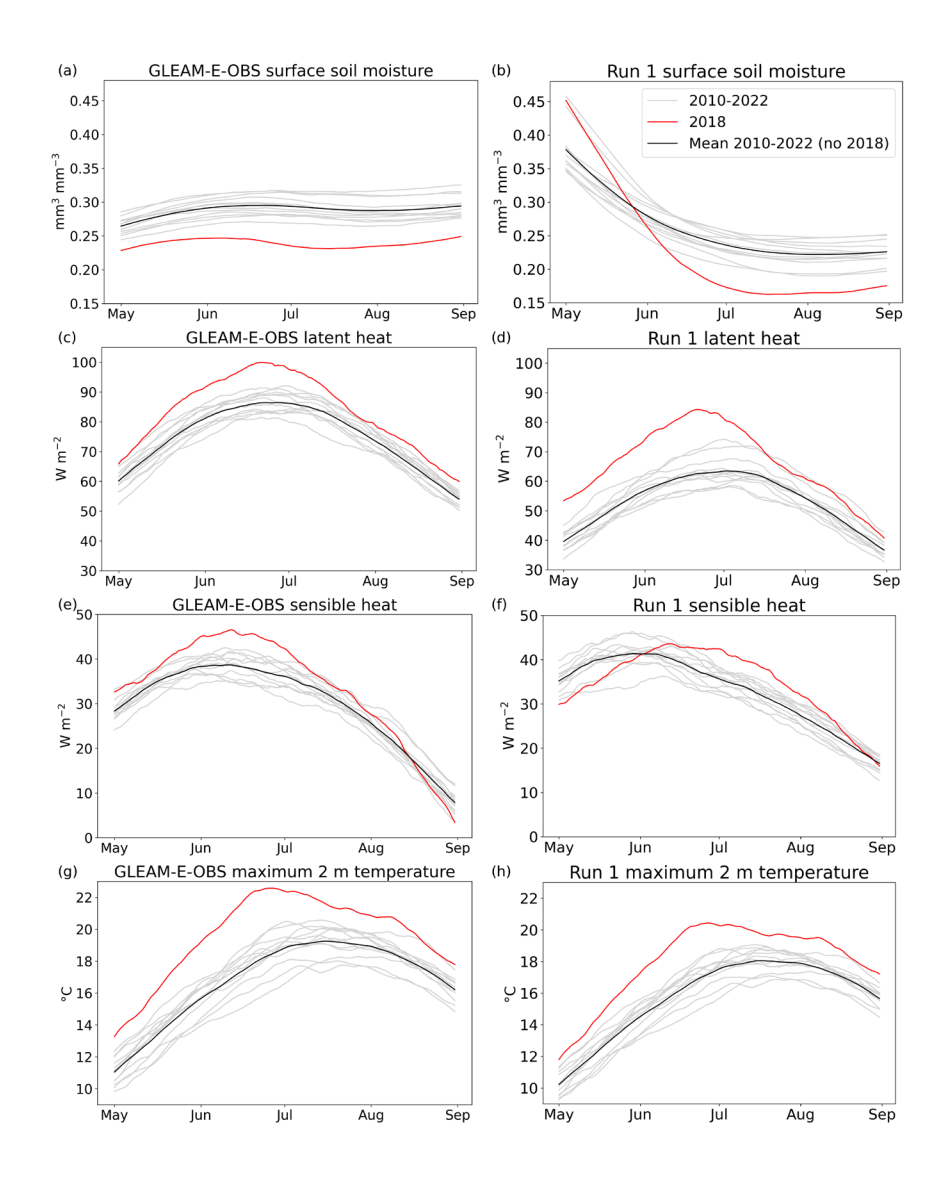


Figure S14. GLEAM-E-OBS (left column) and Run 1 (right column) 92-day centered running mean time series of surface soil moisture, latent heat, sensible heat, and maximum 2 m temperature during MJJA 2010–2022, averaged over the land grid cells in the study domain.

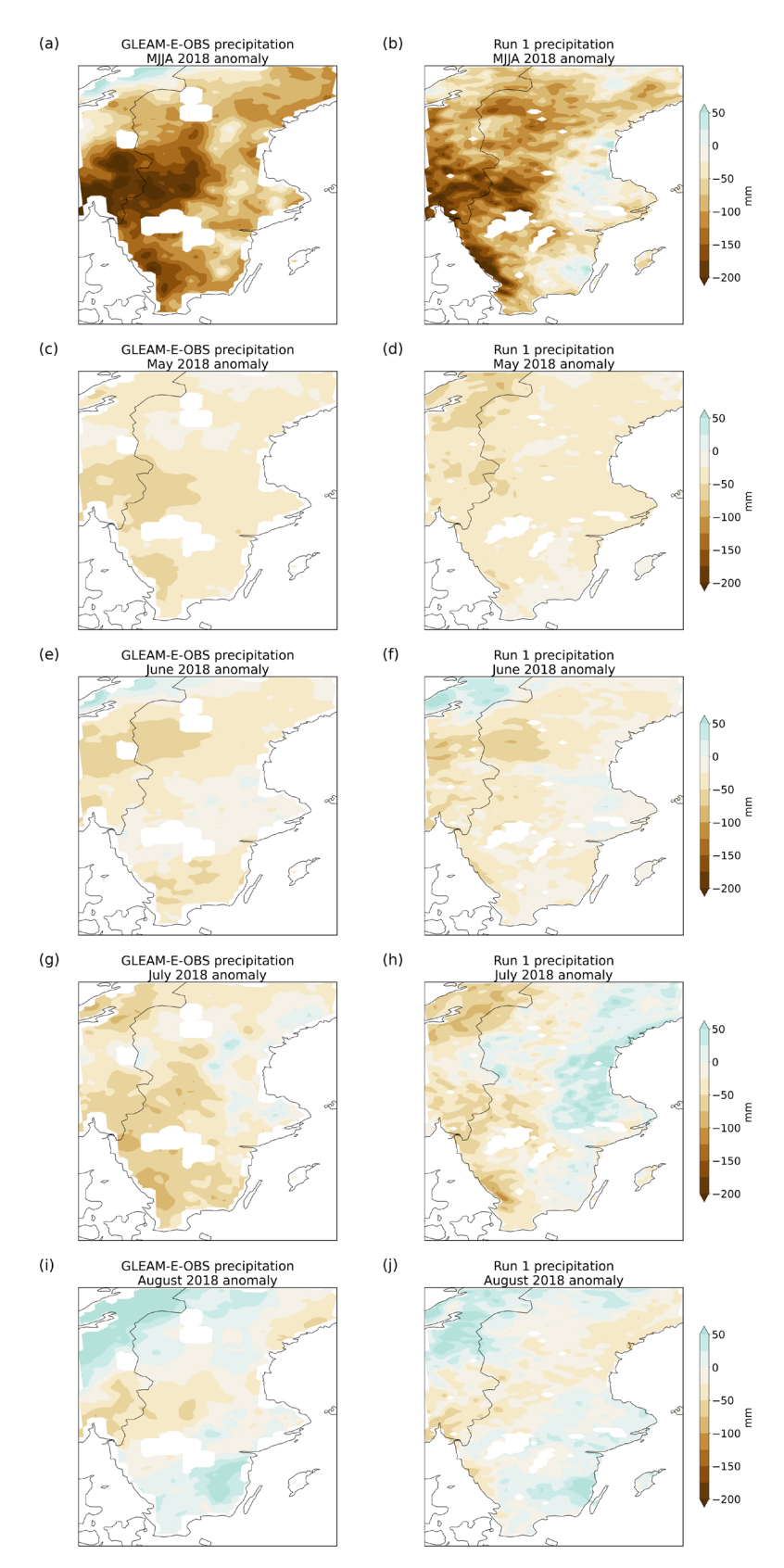


Figure S15. Mean seasonal and monthly May-August anomalies in total precipitation in GLEAM-E-OBS (left column) and Run 1 (right column).

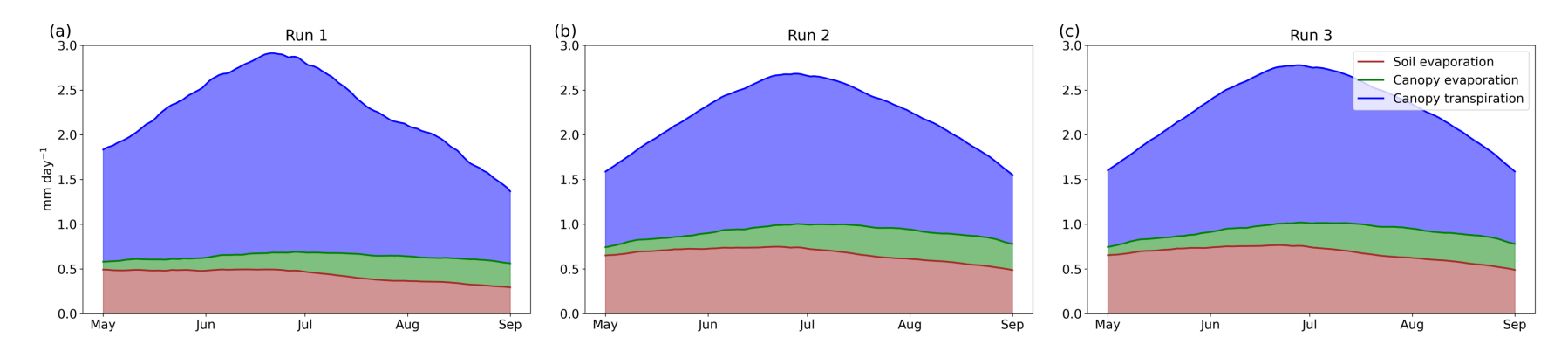


Figure S16. 92-day centered running mean time series of evaporation components in Runs 1–3 during MJJA 2018, averaged over the land grid cells in the study domain. Colored areas represent contributions of different evaporation components to the total evaporation, i.e., the sum of the colored areas at each time step represents total evaporation.

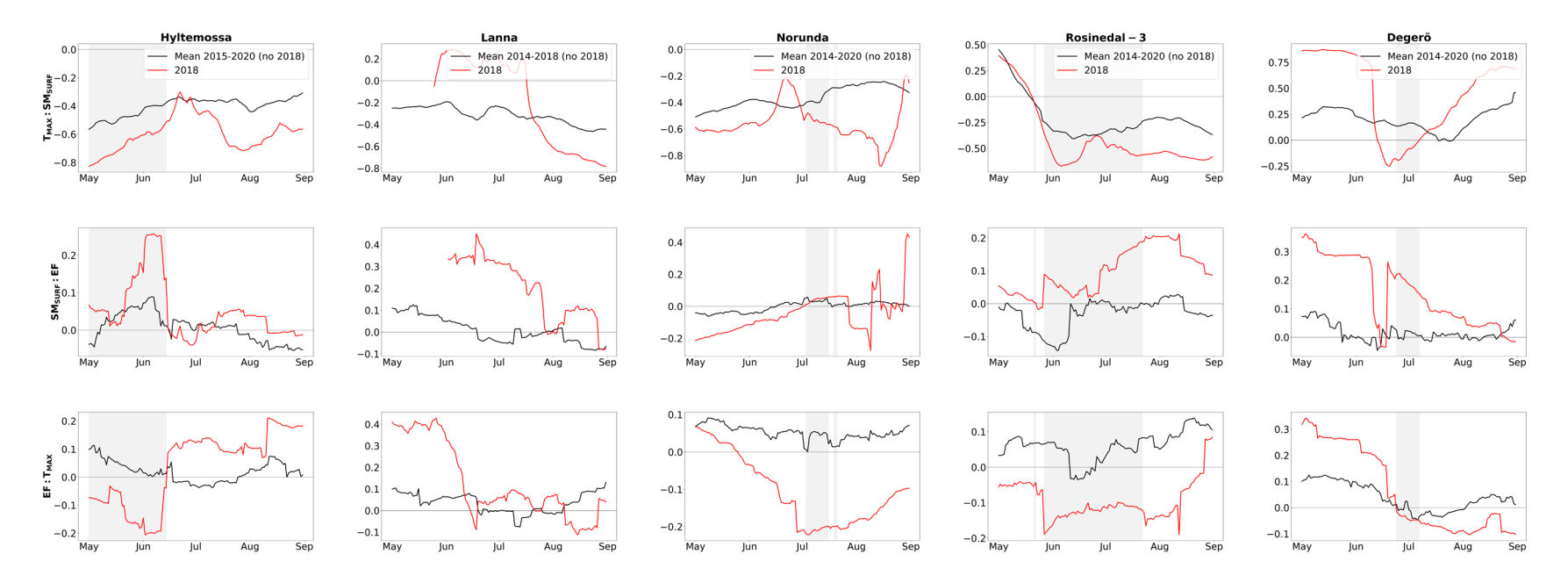


Figure S17. Soil moisture-temperature coupling analysis at the five stations throughout MJJA 2018 and the mean MJJA of other years with available *in situ* data, illustrated as a time series of Pearson correlation coefficients (PCC) based on 92-day (or 10-day as a minimum due to missing data) running periods. The rows demonstrate the coupling components: negative SMsure: TMAX, positive SMsure: EF, and negative EF: TMAX correlations, each occurring simultaneously with an increasing TMAX. The shading denotes periods of complete coupling identified through the multi-correlation overlay approach.

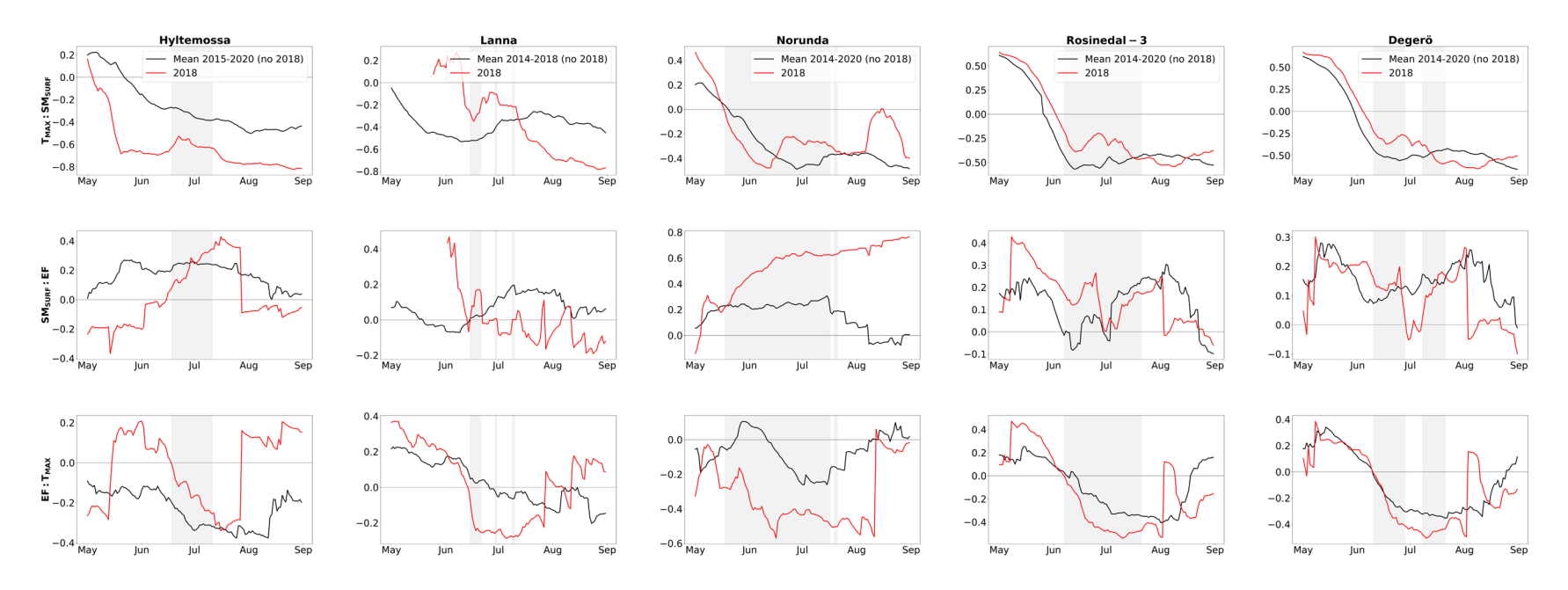


Figure S18. As in Fig. S17, but for GLEAM-E-OBS grid cells. Daily data used to illustrate a time series of Pearson correlation coefficients (PCC) are masked to correspond to the availability of the station's daily data.

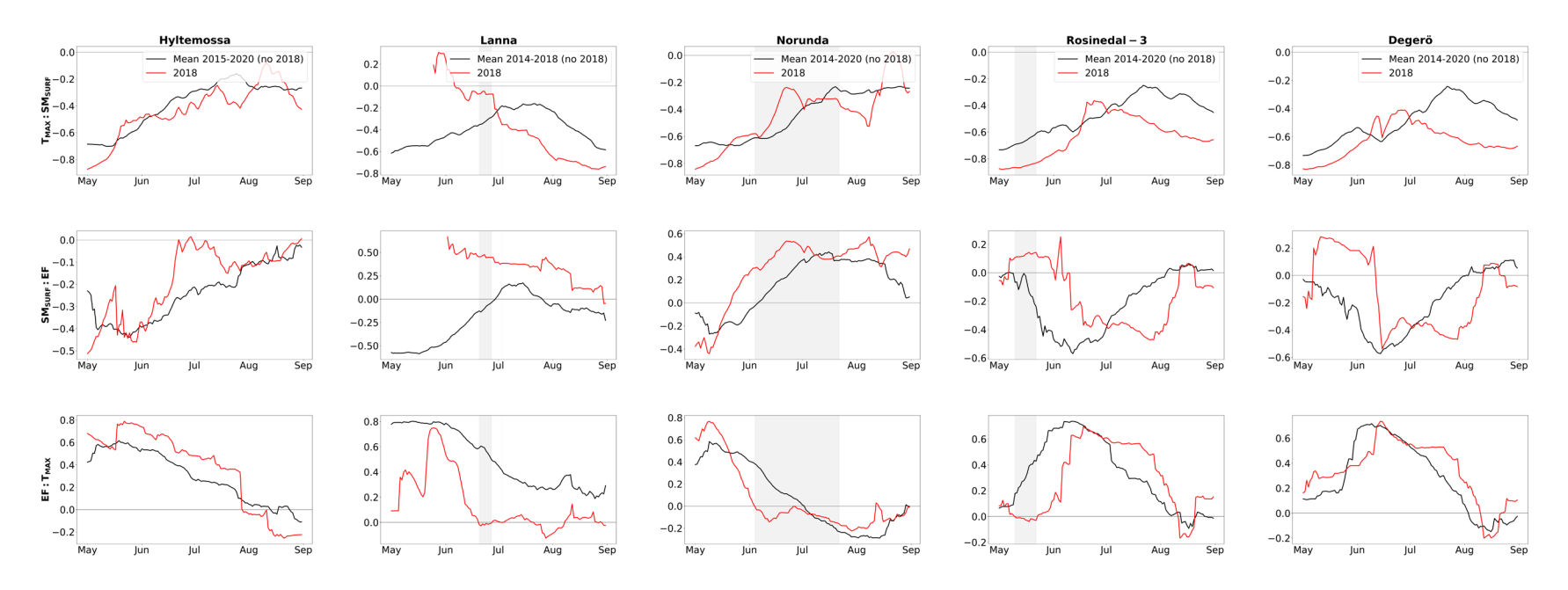


Figure S19. As in Fig. S17, but for Run 1 grid cells. Daily data used to illustrate a time series of Pearson correlation coefficients (PCC) are masked to correspond to the availability of the station's daily data.

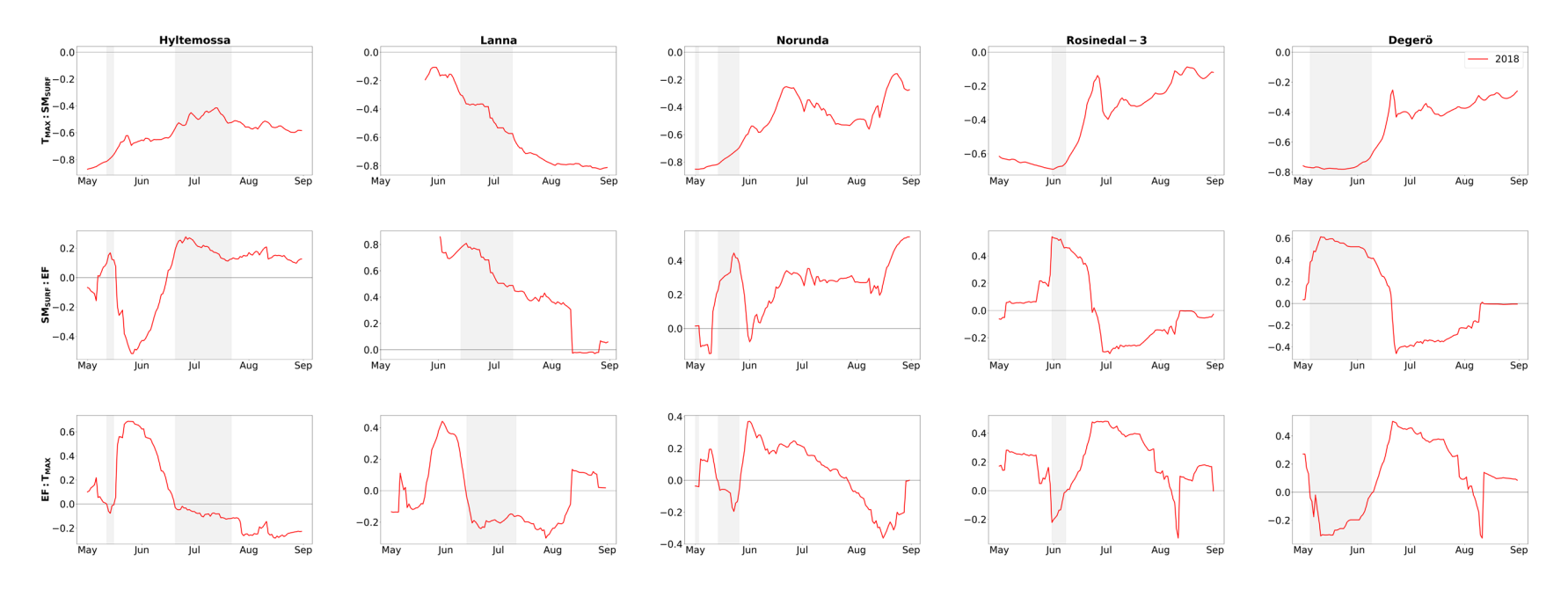


Figure S20. As in Fig. S17, but for Run 2 grid cells. Run 2 only includes the year 2018. Daily data used to illustrate a time series of Pearson correlation coefficients (PCC) are masked to correspond to the availability of the station's daily data.

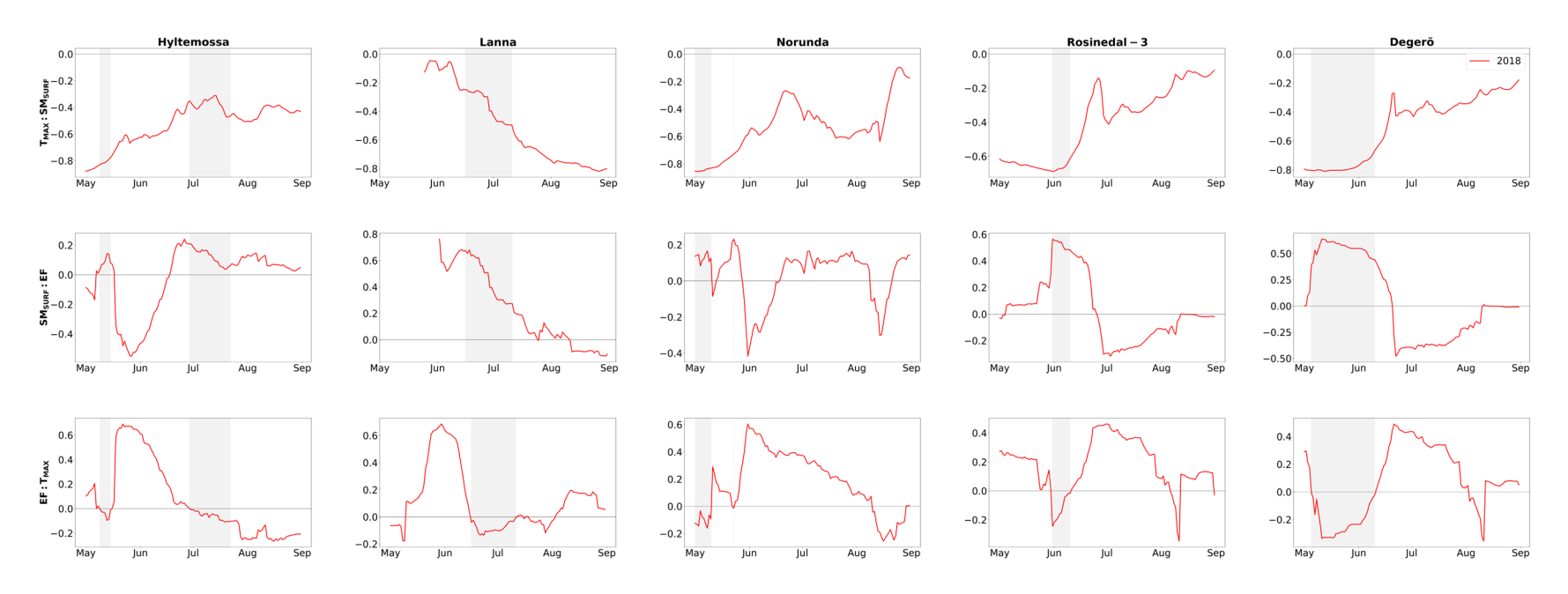


Figure S21. As in Fig. S17, but for Run 3 grid cells. Run 3 only includes the year 2018. Daily data used to illustrate a time series of Pearson correlation coefficients (PCC) are masked to correspond to the availability of the station's daily data.

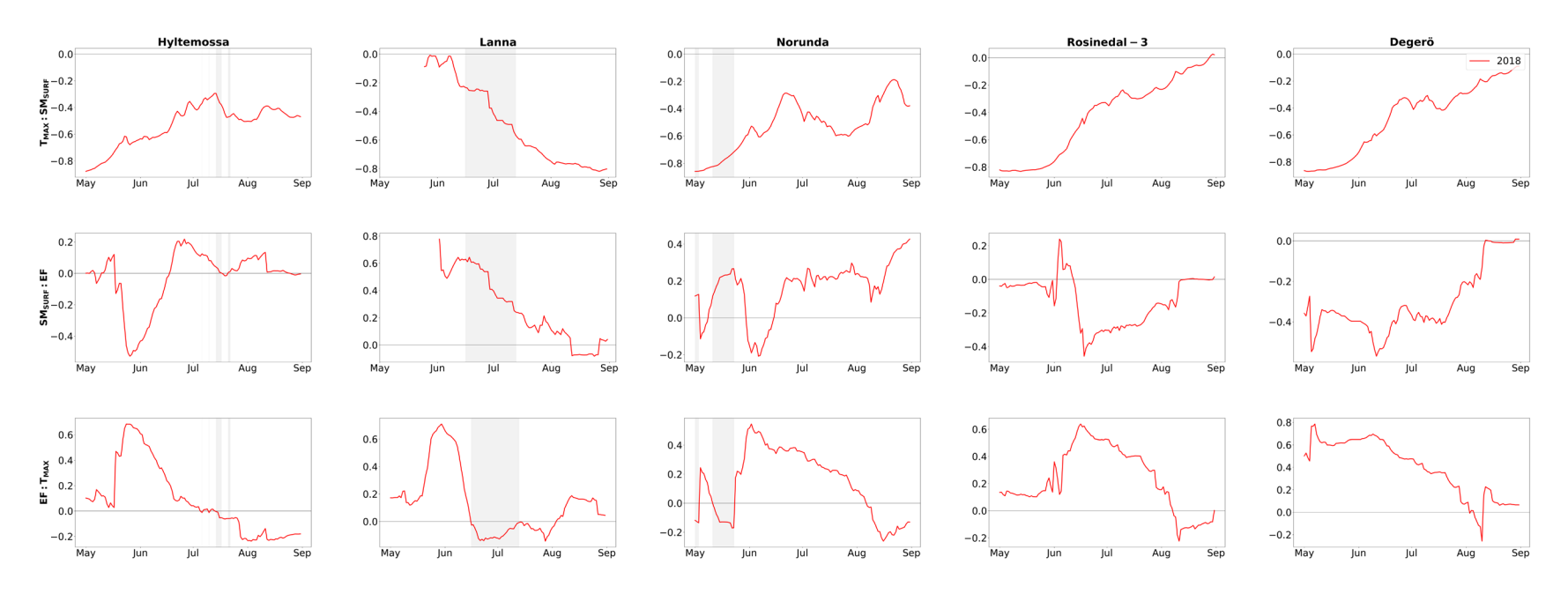


Figure S22. As in Fig. S17, but for Run 4 grid cells. Run 4 only includes the year 2018. Daily data used to illustrate a time series of Pearson correlation coefficients (PCC) are masked to correspond to the availability of the station's daily data.

Table S1. Land surface characteristics at the stations and in WRF-CTSM simulations. This table adheres to Fig. S3 and provides an overview of topography (elevation), the main soil texture, and vegetation types at an *in situ* scale. Station information is from ICOS Sweden (2025).

| Station name | Elevation | | Dominant soil texture types | | Dominant vegetation types | | |
|-----------------|-----------|-------|--|--|--|---|--|
| | Station | Model | Station (uppermost soil layer) | Model (content in the 0-0.1 m soil depth) | Station | Model | |
| Lanna | 75 m | 80 m | Predominant clay content (45% in the 0-30 cm layer) | 43% clay 26% sand | Temperate agriculture | 94.6% grassland, 3.6% needleleaf evergreen forest, 1.8% broadleaf deciduous forest | |
| Norunda | 45 m | 33 m | Sandy-loamy tills with stones and blocks | 47% sand 18% clay | Scots pine and Norway spruce evergreen mixed forest | 77.4% needleleaf evergreen forest, 12.6% broadleaf deciduous forest, 10% grassland | |
| Hyltemossa | 115 m | 111 m | Sandy till surrounded by glaciofluvial sediments | 42% sand 23% clay | Norway spruce evergreen forest | 70.7% needleleaf evergreen forest, 24.4% broadleaf deciduous forest, 4.9% grassland | |
| Rosinedal-3 | 145 m | 228 m | Sand and fine sand | 50% sand 20% clay | Pine forest | 89.8% needleleaf evergreen forest, 9.1% grassland, 1.1% broadleaf deciduous forest | |
| Degerö | 270 m | 215 m | Peatland | 50% sand 20% clay | Boreal mire | 89.9% needleleaf evergreen forest, 8.6% grassland, 1.5% broadleaf deciduous forest | |

Table S2. Ranking summary of the mean MJJA 2018 grid cell evaluation results adopted from Figs. 3 and S4–S8 for surface soil moisture, latent heat, sensible heat, and maximum 2 m temperature. Evaluation metrics are based on daily values and calculated relative to the station data. They include the Pearson correlation coefficient (PCC), root mean square error (RMSE), and absolute bias (AB). E stands for ESA-CCI, G for GLEAM-E-OBS, while the numbers indicate Runs 1–4. Their order in each cell denotes dataset ranking. Surface soil moisture depths are 0.05 m (ESA CCI) and 0.1 m (stations, GLEAM-E-OBS, and Runs 1–4). The rightmost column indicates the dataset with the highest score per location, based on the PCC metric only and based on all evaluation metrics. Underlined entries have the same evaluation results and thus share the same position in the ranking.

| MJJA 2018 | Evaluation metrics | SM_{SURF} | LH | SH | T _{MAX} | The highest score per location |
|----------------------|--------------------------------|-------------------------|----------------|----------------|------------------|--------------------------------|
| | PCC | G4 <u>23</u> 1E | 1G432 | <u>23,41G</u> | <u>1234G</u> | G |
| Mean of all stations | RMSE | G <u>4E,123</u> | <u>24</u> 31G | 2341G | 1 <u>43</u> 2G | |
| | AB | EG4 <u>23</u> 1 | <u>24,31</u> G | 2431G | 1432G | |
| | The highest score per variable | G | 4 | 2 | 1 | - |
| | PCC | <u>EG3</u> 421 | 23 <u>14</u> G | 3421G | G <u>13,24</u> | 3 |
| Hyltemossa | RMSE | <u>34</u> 2 <u>EG</u> 1 | 4 <u>32</u> 1G | 4321G | G1432 | |
| | AB | 342EG1 | 4 <u>32</u> 1G | 4 <u>23</u> 1G | 1432G | |
| | The highest score per variable | 3 | 4 | 4 | G | 4 |
| | PCC | 1 <u>34</u> 2GE | G2 <u>31</u> 4 | 2431G | <u>G1,234</u> | 1 |
| Norunda | RMSE | 12 <u>34</u> GE | 24 <u>3G</u> 1 | 2431G | 1432G | |
| | AB | <u>12,34</u> GE | G1243 | 2 <u>34</u> 1G | 143 <u>2G</u> | |
| | The highest score per variable | 1 | G | 2 | 1 | 1 |
| | PCC | G2314E | 4123G | G <u>23</u> 41 | <u>G23,14</u> | G |
| Rosinedal-3 | RMSE | <u>G1</u> E4 <u>23</u> | 4 <u>23</u> 1G | <u>234</u> G1 | G <u>23</u> 41 | |
| | AB | 1GE4 <u>23</u> | 4321G | 4321G | 4 <u>23</u> G1 | |
| | The highest score per variable | <u>G1</u> | 4 | 4 | G | <u>4G</u> |
| | PCC | GE23 <u>14</u> | 143G2 | 1432G | G <u>1234</u> | <u>1G</u> |
| Lanna | RMSE | EG1 <u>34</u> 2 | 1432G | 4321G | <u>34,21</u> G | |
| | AB | EG1 <u>234</u> | 1243G | 2431G | 4 <u>32</u> 1G | |
| | The highest score per variable | Е | 1 | 4 | 4 | 4 |
| | PCC | E4G132 | 1G432 | 23G41 | G23,14 | G |
| Degerö | RMSE | 4 <u>23,EG</u> 1 | 1G432 | 1G234 | 1 <u>24,G3</u> | |
| | AB | <u>23</u> 4EG1 | 1234G | G2341 | 14 <u>23</u> G | |
| | The highest score per variable | 4 | 1 | <u>G2</u> | 1 | 1 |

Table S3. As in Table S2, but for July 2018. Grid cell evaluation figures illustrating WRF-CTSM simulations and GLEAM-E-OBS dataset against *in situ* observations only for July 2018 are not included in the Supplement.

| July 2018 | Evaluation metrics | SM_{SURF} | LH | SH | T_{MAX} | The highest score per location |
|----------------------|--------------------------------|-----------------|----------------|----------------|----------------|--------------------------------|
| | PCC | 123E4G | 1G <u>43</u> 2 | 1G <u>42</u> 3 | G <u>1234</u> | 1 |
| Mean of all stations | RMSE | <u>G23,E4</u> 1 | <u>12</u> 43G | 2431G | 4 <u>13</u> 2G | |
| | AB | <u>G2,E34</u> 1 | 1243G | 2 <u>34,1G</u> | 4 <u>13</u> 2G | |
| | The highest score per variable | G | 1 | 2 | 4 | - |
| | PCC | G24 <u>E3</u> 1 | 234G1 | <u>43</u> 21G | <u>43G,12</u> | 3 |
| Hyltemossa | RMSE | <u>234</u> 1EG | <u>34</u> 21G | <u>234</u> 1G | 4312G | |
| | AB | <u>23</u> 41EG | <u>234</u> 1G | 2 <u>34</u> 1G | 4 <u>31</u> 2G | |
| | The highest score per variable | 2 | <u>23</u> | <u>234</u> | 4 | 2 |
| | PCC | 32G41E | G3214 | 214G3 | G <u>234</u> 1 | G |
| Norunda | RMSE | <u>12</u> 34GE | G2143 | <u>21</u> 43G | G4132 | |
| | AB | 12 <u>34</u> GE | G2143 | <u>21</u> 43G | 143G2 | |
| | The highest score per variable | 1 | G | 2 | G | G |
| | PCC | 1G23E4 | G1234 | G3241 | <u>G3,24</u> 1 | G |
| Rosinedal-3 | RMSE | 1GE <u>23</u> 4 | G <u>43</u> 21 | <u>3G,24</u> 1 | G3 <u>24</u> 1 | |
| | AB | 1GE <u>23</u> 4 | G4321 | 342G1 | <u>23,G4</u> 1 | |
| | The highest score per variable | 1 | G | 3 | <u>G3</u> | <u>G3</u> |
| | PCC | 234G1E | 2341G | 4321G | G <u>43</u> 12 | 2 |
| Lanna | RMSE | EG1 <u>234</u> | <u>234</u> 1G | 4231G | <u>43,G2</u> 1 | |
| | AB | EG1 <u>234</u> | 2143G | 2431G | <u>43</u> 21G | |
| | The highest score per variable | Е | 2 | 4 | <u>43</u> | 4 |
| Degerö | PCC | EG4231 | 2431G | G2314 | G <u>234</u> 1 | G |
| | RMSE | 4 <u>23</u> EG1 | G <u>34</u> 21 | G2341 | 14 <u>23</u> G | |
| | AB | 4 <u>23</u> EG1 | 4G321 | G2 <u>34</u> 1 | 14 <u>23</u> G | |
| | The highest score per variable | 4 | 4 | G | 1 | 4 |

Table S4. As in Table S3, but for precipitation in MJJA and July 2018. NaN for all indicates that the Pearson correlation coefficient (PCC) against *in situ* precipitation data is undefined, given that no precipitation was recorded at Hyltemossa station throughout the entire month of July.

| Precipitation (MJJA and July 2018) | Evaluation metrics | MJJA 2018 | The highest score per location (MJJA 2018) | July 2018 | The highest score per location (July 2018) | |
|------------------------------------|--------------------------------|-----------------------|--|----------------|--|--|
| | PCC | 1G234 | 1 | 1G234 | 1 | |
| Mean of all stations | RMSE | 1G324 | | 12 <u>G3</u> 4 | | |
| | AB | <u>34,G2</u> 1 | | 31 <u>24</u> G | | |
| | The highest score per variable | | 1 | | 1 | |
| | PCC | 1G342 | 1 | (NaN for all) | - | |
| Hyltemossa | RMSE | 1G <u>34</u> 2 | | 1G342 | | |
| Hyliciliossa | AB | 1 <u>G4</u> 32 | | <u>G1,34</u> 2 | | |
| | The highest score per variable | | 1 | | <u>G1</u> | |
| | PCC | G2134 | G | G2134 | G | |
| Norunda | RMSE | G2134 | | G2143 | | |
| Norunda | AB | <u>13</u> G24 | | G3142 | | |
| | The highest score per variable | | G | G | | |
| | PCC | 42 <u>13</u> G | 4 | <u>24</u> 31G | 4 | |
| Rosinedal-3 | RMSE | 42 <u>13</u> G | | 4231G | | |
| Kosilicuai-3 | AB | <u>24</u> 3 <u>G1</u> | | 4123G | | |
| | The highest score per variable | 4 | | 4 | | |
| | PCC | G1432 | G | G4321 | G | |
| Lanna | RMSE | G1 <u>42</u> 3 | | G1423 | | |
| | AB | 1243G | | 12 <u>34G</u> | | |
| | The highest score per variable | | G | | G | |
| | PCC | G1432 | G | 1 <u>34</u> 2G | 1 | |
| Dagarö | RMSE | <u>G1,43</u> 2 | | 13 <u>24</u> G | | |
| Degerö | AB | <u>G34,12</u> | | G1342 | | |
| | The highest score per variable | | G | | 1 | |

Supplementary references

Allen, R. G., Luis S. Pereira, Dirk Raes, and Martin Smith: Crop evapotranspiration: guidelines for computing crop water requirements, Food and Agriculture Organization of the United Nations, Rome, 300 pp., 1998.

Dirmeyer, P. A., Balsamo, G., Blyth, E., Morrison, R., and Cooper, H. M.: Land-Atmosphere Interactions Exacerbated the Drought and Heatwave over Northern Europe during Summer 2018, AGU Adv., 2, e2020AV000283, https://doi.org/10.1029/2020AV000283, 2021.

Global Soil Data Task: Global Soil Data Products CD-ROM Contents (IGBP-DIS). International Geosphere-Biosphere Programme-Data and Information Available Services, https://doi.org/10.3334/ORNLDAAC/565, 2000.

ICOS Sweden: https://www.icos-sweden.se/, last access: 26 February 2025.

Lawrence, P. J. and Chase, T. N.: Representing a new MODIS consistent land surface in the Community Land Model (CLM 3.0), J. Geophys. Res., 112, G01023, https://doi.org/10.1029/2006JG000168, 2007.

Verdin, K. L. and Greenlee, S. K.: Development of continental scale digital elevation models and extraction of hydrographic features, in: Proceedings, Third International Conference/Workshop on Integrating GIS and Environmental Modeling, Santa Fe, New Mexico, 1996.